

Adaption of 3D Models to 2D X-Ray Images during Endovascular Abdominal Aneurysm Repair

Daniel Toth^{1,2}, Marcus Pfister¹, Andreas Maier², Markus Kowarschik¹,
and Joachim Hornegger²

¹ Siemens Healthcare GmbH, Forchheim, Germany

² Pattern Recognition Lab., Friedrich-Alexander-University Erlangen-Nuremberg,
Erlangen, Germany

Abstract. Endovascular aneurysm repair (EVAR) has been gaining popularity over open repair of abdominal aortic aneurysms (AAAs) in the recent years. This paper describes a distortion correction approach to be applied during the EVAR cases. In a novel workflow, models (meshes) of the aorta and its branching arteries generated from preoperatively acquired computed tomography (CT) scans are overlaid with interventionally acquired fluoroscopic images. The overlay provides an arterial roadmap for the operator, with landmarks (LMs) marking the ostia, which are critical for stent placement. As several endovascular devices, such as angiographic catheters, are inserted, the anatomy may be distorted. The distortion reduces the accuracy of the overlay. To overcome the mismatch, the aortic and the iliac meshes are adapted to a device seen in uncontrasted intraoperative fluoroscopic images using the skeleton-based as-rigid-as-possible (ARAP) method. The deformation was evaluated by comparing the distance between an ostium and the corresponding LM prior to and after the deformation. The central positions of the ostia were marked in digital subtraction angiography (DSA) images as ground truth. The mean Euclidean distance in the image plane was reduced from 19.81 ± 17.14 mm to 4.56 ± 2.81 mm.

Keywords: computational geometry, as-rigid-as-possible, mesh deformation, abdominal aortic aneurysm, EVAR.

1 Introduction

The abdominal aortic aneurysm (AAA) is one of the most frequent aortic diseases. It is a dilatation of the abdominal aorta. AAAs, such as cardiac diseases, are becoming increasingly more common due to the continuous aging of the population. In the case of aneurysm rupture, 60% of the patients reach the hospital alive and 65% of these patients die during elective repair [1]. Detection of AAAs prior to rupture is challenging. They are mostly asymptomatic, thus often found accidentally. If the aneurysm diameter exceeds 5.5 cm or its expansion is rapid, it is decided for elective repair [9]. Endovascular aneurysm repair (EVAR) represents a more novel approach than open surgery. During an EVAR intervention,

the operating physician inserts endovascular instruments through minor incisions at the groins and places a stent graft into the body of the aneurysm to exclude the weakened wall of the aorta from the blood flow. EVAR causes less trauma to the patient and the recovery times are significantly shorter compared to open repair. There is no difference in long-term mortality rates, but the short-term death rate of EVAR is significantly lower [10].

EVAR procedures are navigated by X-ray fluoroscopic images. To visualize vascular structures during the intervention, iodinated contrast agent is injected. However, as the patients are in advanced age, their renal functions may not be sufficient to process the injected contrast medium. In a more novel workflow, a preoperatively acquired computed tomography (CT) volume is segmented [8]. The resulting surface meshes of the aorta and the branching arteries are used for preinterventional planning. Landmarks (LMs) of the main branching artery ostia are calculated automatically and the physician may set further LMs manually. After the LM calculation, optimal angulations of the interventional C-arm system are calculated to be recalled during the intervention.

During the intervention, the preoperative CT dataset is registered to the C-arm system [2] and the mesh models of the aorta and its branching arteries are projected onto the fluoroscopic images which provides an arterial roadmap for the operator and potentially leads to a reduction in contrast agent load. However, the inserted endovascular devices may distort the anatomy and reduce the accuracy of the overlay. To compensate for the mismatch, several approaches have been developed previously. Non-rigid registration approaches were implemented by Liao et al. [7] and Guyot et al. [3], which require intense contrast agent usage. Another approach is based on the implementation of a finite element method (FEM) [6]. The FEM has a high computational complexity and current implementations only simulate the deformation prior to the intervention.

In this paper, the application of the skeleton-based variant of the as-rigid-as-possible (ARAP) mesh deformation for endovascular distortion correction is presented. The ARAP method was developed by Igarashi et al. for 2D surface deformations [5] and reformulated by Sorkine and Alexa to handle 3D surface meshes [11]. The 3D ARAP method can be considered as the successor of the Laplacian surface editing method developed by Sorkine et al. [12]. The 3D surface mesh ARAP framework was extended by Zhang et al. with a skeletal constraint to result in better volume preservation [13]. We implemented this skeleton-based variant of the ARAP surface mesh deformation with a control point selection and transformation algorithm. The evaluation revealed that the implemented method was able to increase the accuracy of the arterial roadmap significantly in the case of anatomical distortion.

2 Methods

The idea is to adapt the mesh model to the reconstructed 3D device such that it smoothly deforms to the new position. Due to the knowledge of the position of the 3D device, the new position of some of the vertices can be determined. Due

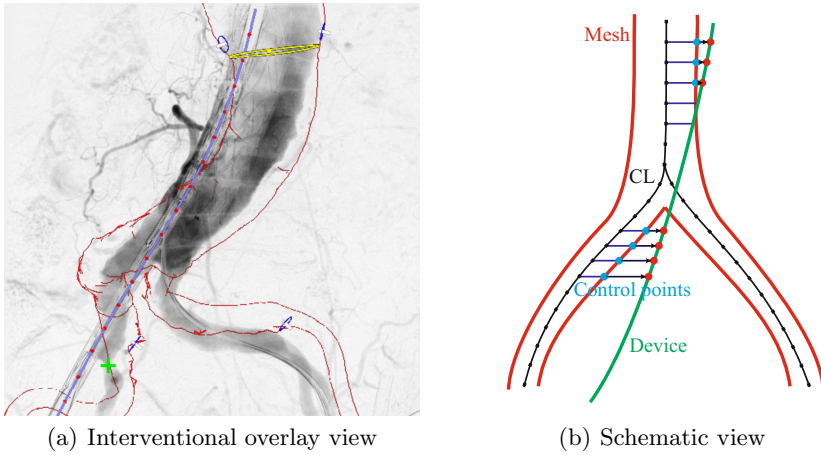


Fig. 1. (a) The interventional view shows an overlay of a preoperative CT and a DSA image with the reconstructed device. (b) Rays are cast between the mesh centerline (CL) and the device. If a ray hits the mesh, the hit point is designated as a control point, which will be moved to the device points.

to anatomical constraints, the position of some other vertices can be fixed. The known vertices represent the control points of the applied method, see Figure 1.

The ARAP method ensures that the deformed shape matches the control points on one hand and, on the other hand, the remaining vertices are displaced with as minimal transformations as possible.

2.1 Skeleton-Based As-Rigid-As-Possible Mesh Deformation

A triangular surface mesh, in the following shape \mathcal{S} , is characterized by its vertices $\mathbf{v}_i \in \mathbb{R}^3$ and edges $\mathbf{e}_{ij} = \mathbf{v}_i - \mathbf{v}_j$ connecting the vertices. A deformed surface mesh is denoted by \mathcal{S}' in the following, with deformed vertex positions \mathbf{v}'_i and deformed edges \mathbf{e}'_{ij} . Shapes \mathcal{S} and \mathcal{S}' may have different geometries, but must have the same topology after deformation.

For the non-rigid deformation between the shapes \mathcal{S} and \mathcal{S}' , an energy function was formulated by Sorkine and Alexa [11]:

$$E(\mathcal{S}, \mathcal{S}') = \sum_{i=1}^n \sum_{j \in \mathcal{N}(i)} w_{ij} \|\mathbf{e}'_{ij} - \mathbf{R}_i \mathbf{e}_{ij}\|_2^2, \quad (1)$$

where n denotes the number of vertices, the w_{ij} represent edge weights and \mathbf{R}_i denotes the rotation matrix of a cell, i.e., the vertex \mathbf{v}_i and its one-ring neighborhood $\mathcal{N}(i)$. To compensate for possible mesh non-uniformities, the w_{ij} were chosen to be cotangent weights [11]. This formulation guarantees maximal

rigidity, if optimized for minimal rotations. The minimization and reordering results for all vertices i in

$$\sum_{j \in \mathcal{N}(i)} w_{ij}(\mathbf{v}'_i - \mathbf{v}'_j) = \sum_{j \in \mathcal{N}(i)} \frac{w_{ij}}{2}(\mathbf{R}_i + \mathbf{R}_j)(\mathbf{v}_i - \mathbf{v}_j) \implies \mathbf{L}\mathbf{v}' = \mathbf{b}(\mathbf{R}), \quad (2)$$

where \mathbf{L} is a weighted Laplacian matrix and $\mathbf{b}(\mathbf{R})$ denotes the right hand side of the resulting linear system of equations depending on the local rotations.

The ARAP transformation is controlled by a subset of vertices with known new positions. These positions may either be kept identical to their previous ones (anchor points) or transformed into explicitly defined new ones (handle points). The union of these designated vertices is called control points. In [12] these m control points \mathbf{v}_{c_i} are taken into account in the previously derived Laplacian surface editing energy formulation

$$E_L(\mathcal{S}, \mathcal{S}') = \|\mathbf{L}\mathbf{v}' - \delta\|_2^2 + \sum_{i=1}^m \|\mathbf{v}'_{c_i} - \mathbf{v}_{c_i}\|_2^2 \implies \mathbf{L}\mathbf{v}' = \mathbf{b}, \quad (3)$$

where $\delta = \mathbf{L}\mathbf{v}$.

The similarity between Equation 2 and Equation 3 is apparent. The control point constraint can easily be added to the ARAP energy formulation and system matrix as well. The left hand side, the system matrix, is identical, but the right hand side is dependent on the local rotations \mathbf{R}_i in the ARAP method.

The linear system of equations of the ARAP approach can be solved with a two-step iteration. Prior to the iteration, the edge weights w_{ij} are computed and the system matrix \mathbf{L} is assembled and prefactorized. As the matrix \mathbf{L} is sparse, symmetric and positive definite, a sparse Cholesky decomposition, as proposed in [11], is used. Next, an initial guess, the Laplacian surface editing solution, $\mathbf{v}'_{(0)}$ is calculated by solving Equation 2 with all rotations \mathbf{R}_i set to identity.

In the first step, the iteration calculates the optimal local rotations \mathbf{R}_i by minimizing Equation 1 with the calculated previous solution $\mathbf{v}'_{(0)}$. In the second step, the rotations \mathbf{R}_i are substituted into the right hand side of Equation 2 and the next solution $\mathbf{v}'_{(1)}$ is calculated by solving the equation system. These two iteration steps are repeated until convergence.

We implemented the extended ARAP framework developed by Zhang et al. to account for possible volume deflations [13]. For volume preservation, a skeletal constraint was incorporated. The constraint can be formulated as an additional term in the Laplacian energy function:

$$E_{skel}(\mathcal{S}, \mathcal{S}') = \|\mathbf{L}\mathbf{v}' - \delta\|_2^2 + \|\mathbf{L}_s \mathbf{v}'_{all} - \delta_s\|_2^2 + \sum_{i=1}^m \|\mathbf{v}'_{c_i} - \mathbf{v}_{c_i}\|_2^2, \quad (4)$$

where \mathbf{L}_s denotes the Laplacian matrix of the skeleton points, $\mathbf{v}'_{all} = [\mathbf{v}', \mathbf{v}'_s]^T$ with \mathbf{v}'_s as the added skeleton points and $\delta_s = \mathbf{L}_s \mathbf{v}_{all}$. In matrix form, this reads

$$\begin{bmatrix} \mathbf{L} & | & \mathbf{0} \\ \mathbf{I}_c & | & \mathbf{0} \\ & & \mathbf{L}_s \end{bmatrix} \begin{bmatrix} \mathbf{v}' \\ \mathbf{v}'_s \end{bmatrix} = \begin{bmatrix} \delta \\ \mathbf{v}_c \\ \delta_s \end{bmatrix}, \quad (5)$$

where \mathbf{I}_c denotes the mapping between \mathbf{v} and \mathbf{v}_c .

The additional rows in the system matrix do not increase the computational complexity significantly, as $m \ll n$. The resulting linear system of equations can be solved by applying the previously described two-step iterative scheme.

2.2 Control Point Selection

To determine whether and where to deform the aortic or an iliac surface mesh, rays are cast from the centerline of the vessel mesh to the reconstructed endovascular device in 3D. If a cast ray hits the mesh, this indicates that the device line is outside of the mesh, thus the mesh has to be deformed around the hit point \mathbf{h} . The hit point is selected as a handle point and its shift \mathbf{s} is calculated by

$$\mathbf{s} = \mathbf{d} - \mathbf{h} + \Delta d \frac{(\mathbf{d} - \mathbf{h})}{\|\mathbf{d} - \mathbf{h}\|}, \quad (6)$$

where \mathbf{d} denotes the respective device point and Δd represents the device thickness. In case of tortuous vessels, a resampling of the control points is performed to ensure a more equally distributed sampling. To account for the large flexibility of the abdominal aorta, no anchor points were defined explicitly.

2.3 Mesh Deformation

The aortic and iliac meshes are deformed independently of each other. First, the inserted device is reconstructed in 3D from two views [4]. Next, the control points for the aortic and the iliac mesh to be deformed are defined.

As the skeleton-based ARAP deformation is used, a skeleton has to be generated, which is simple as the vessel meshes are rather tubular. Each mesh is sliced by planes every 5 mm along the centerline perpendicular to it. Along each slicing plane, six equiangular rays are cast. The ray-mesh hit points are defined as skeleton points. First, the aortic mesh is deformed by translating the control points and executing the two-step iteration. Second, the selected iliac mesh is deformed by translating its control points by the calculated shifts, and the top control points are moved to the previously found nearest aortic vertices. After the deformation, the vertices of the aortic mesh below the bound iliac points are erased for the sake of consistency. The complete deformation (prefactorization and iteration) is performed within one second for a typical mesh size of 7500 vertices on an Intel i7 - 3720QM with 8 GB RAM.

3 Results and Evaluation

3.1 Data Description

The evaluation of the implemented method was performed on real clinical data. The data was provided by two clinical collaboration sites, Universitätsklinikum Heidelberg (HD) and Centre Hospitalier de l'Université de Montréal (CHUM).

Each of the datasets covered a CT volume with sufficient quality for segmentation, data for registration and DSA images of the iliac bifurcation. Optimally, each patient has two 2D images of each iliac bifurcation to be able to reconstruct the endovascular device in 3D. 17 datasets with 31 distinct DSA images (excluding images for device reconstruction) were found eligible for evaluation.

3.2 Qualitative Results

First, the deformation was evaluated qualitatively by clinical experts. The segmented models were registered to the renal arteries and the overlay images before and after the deformation were compared visually. As the aorta is rather stiff, the deformation is mostly minor. The deformation corrects for the distortion of the anatomy by the device, while preserving the LM positions, such as those of the renals. The correspondence between the deformed mesh and the contrast agent flow in the DSA images is higher.

In the case of the highly tortuous iliac arteries, even larger improvements can be observed. The part of the reconstructed devices located outside of the mesh is mostly larger than in the aortic case. The distances between the internal iliac artery LMs and the observed ostium positions may also be larger. The overlaid deformed meshes show high correspondence to the contrast agent flow in the DSA images. The new LM positions also show an improvement, see Figure 2.

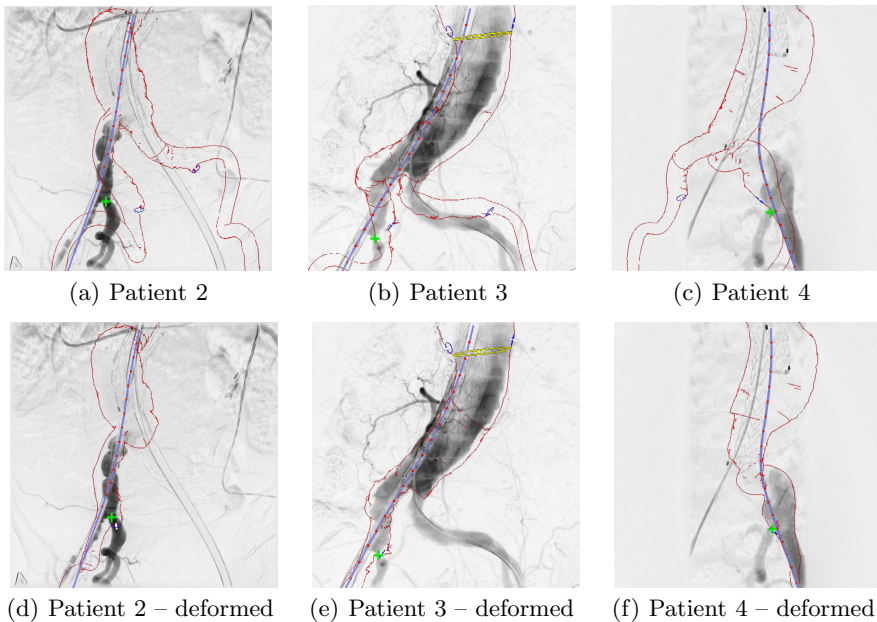


Fig. 2. Iliac overlay images of three patients before (a)(b)(c) and after distortion correction (d)(e)(f) by the skeleton-based ARAP deformation method. Medical data courtesy of HD and CHUM.

3.3 Quantitative Results

The visual impressions of the qualitative evaluation were also proven by quantitative measures. Since there is no possibility to evaluate in 3D, the central positions of the internal iliac artery ostia were marked in the 2D DSA images as ground truth. The corresponding projections of the LM positions were compared to the ground truth prior to and after the deformation, see Table 1.

First, the Euclidean distances between the ostia and the corresponding LMs were measured. The mean initial (undeformed) distance between the ostia and the corresponding LMs was 19.81 mm with a standard deviation of 17.14 mm. After deformation, the mean distance was reduced to 4.56 mm and the standard deviation to 2.81 mm. The median was initially slightly lower than the mean and was also reduced significantly from 15.79 mm to 3.65 mm.

As the characteristic direction of the iliac arteries is vertical, during stent placement the height of the stent endings is critical. Thus, a second distance measure, the vertical distance (difference of z -coordinates), was also considered. The mean initial distance was 11.33 mm with a standard deviation of 8.21 mm. It was reduced to 2.73 mm with a standard deviation of 2.20 mm.

Table 1. Distances between ostia and the corresponding LMs.

	Euclidean dist.		Vertical dist.	
	Initial	Deformed	Initial	Deformed
Mean (mm)	19.81	4.56	11.33	2.73
Std. dev. (mm)	17.14	2.81	8.21	2.20
Median (mm)	15.79	3.65	9.33	2.25

4 Conclusion and Outlook

This paper proposes an approach towards distortion correction during endovascular AAA repair procedures. The method accounts for distortions caused by inserted endovascular devices by adapting the segmented models of the aorta and the iliac arteries using the skeleton-based ARAP mesh deformation. Evaluation shows that the distortion correction increases the accuracy of the overlay of the projected surface meshes with interventionally acquired fluoroscopic images.

The method could be extended to account for multiple inserted devices, thus increasing the accuracy of the deformation. Additionally, both iliacs may be deformed simultaneously. Furthermore, the range of applications can be extended by applying the method for thoracic aortic aneurysm (TAA) repairs.

Acknowledgements and Disclaimer. The authors gratefully acknowledge the help of the group of Prof. Dr. med. D. Böckler from HD, the group of Dr. G. Soulez MD, Msc from CHUM and the group of Dr. med M. Austermann from the Universitätsklinikum Münster for providing the clinical data and evaluating qualitatively. The concepts and information presented in this paper are based on research and are not commercially available.

References

1. Basnyat, P.S., Biffin, A.H.B., Moseley, L.G., Hedges, A.R., Lewis, M.H.: Mortality from ruptured abdominal aortic aneurysm in wales. *British Journal of Surgery* 86(6), 765–770 (1999)
2. Douane, F., Kauffmann, C., Thérassé, E., Lessard, S., Beaudouin, N., Blair, J.F., Oliva, V., Pfister, M., Soulez, G.: Accuracy of rigid registration between CT angiography and fluoroscopy during endovascular repair of abdominal aortic aneurysm (AAA). In: Haage, P., Morgan, R.A. (eds.) CIRSE, Barcelona, Spain, September 14–18 (2013)
3. Guyot, A., Varnavas, A., Carrell, T., Penney, G.: Non-rigid 2D-3D registration using anisotropic error ellipsoids to account for projection uncertainties during aortic surgery. In: Mori, K., Sakuma, I., Sato, Y., Barillot, C., Navab, N. (eds.) MICCAI 2013, Part III. LNCS, vol. 8151, pp. 179–186. Springer, Heidelberg (2013)
4. Hoffmann, M., Brost, A., Jakob, C., Bourier, F., Koch, M., Kurzydum, K., Hornegger, J., Strobel, N.: Semi-automatic catheter reconstruction from two views. In: Ayache, N., Delingette, H., Golland, P., Mori, K. (eds.) MICCAI 2012, Part II. LNCS, vol. 7511, pp. 584–591. Springer, Heidelberg (2012)
5. Igarashi, T., Moscovich, T., Hughes, J.F.: As-rigid-as-possible shape manipulation. *ACM Transactions on Graphics (TOG)* 24(3), 1134–1141 (2005)
6. Kaladji, A., Dumenil, A., Castro, M., Cardon, A., Becquemain, J.-P., Bou-Saïd, B., Lucas, A., Haigron, P.: Prediction of deformations during endovascular aortic aneurysm repair using finite element simulation. *Computerized Medical Imaging and Graphics* 37(2), 142–149 (2013)
7. Liao, R., Tan, Y., Sundar, H., Pfister, M., Kamen, A.: An efficient graph-based deformable 2D/3D registration algorithm with applications for abdominal aortic aneurysm interventions. In: Liao, H., Edwards, P.J.E., Pan, X., Fan, Y., Yang, G.-Z. (eds.) MIAR 2010. LNCS, vol. 6326, pp. 561–570. Springer, Heidelberg (2010)
8. Pfister, M., Toth, D.: Clinical prototype of an integrated workflow for EVAR using surface meshes of pre-operative CT data. In: *Proceedings of the 1st Conference on Image-Guided Interventions* (2014)
9. Sakalihan, N., Limet, R., Defawe, O.D.: Abdominal aortic aneurysm. *The Lancet* 365(9470), 1577–1589 (2005)
10. Schanzer, A., Messina, L.: Two decades of endovascular abdominal aortic aneurysm repair: Enormous progress with serious lessons learned. *Journal of the American Heart Association* 1(3), e000075 (2012)
11. Sorkine, O., Alexa, M.: As-rigid-as-possible surface modeling. In: *Proceedings of the Fifth Eurographics Symposium on Geometry Processing*, Barcelona, Spain, July 4–6, pp. 109–116 (2007)
12. Sorkine, O., Cohen-Or, D., Lipman, Y., Alexa, M., Rössl, C., Seidel, H.: Laplacian surface editing. In: *Second Eurographics Symposium on Geometry Processing*, Nice, France, July 8–10, pp. 175–184 (2004)
13. Zhang, S., Nealen, A., Metaxas, D.: Skeleton based as-rigid-as-possible volume modeling. *Eurographics 2010–Short Papers*, pp. 21–24 (2010)